# EID-based Load Frequency Control for Interconnected Hybrid Power System Integrated with RESs

Fang Liu, *Senior Member*, *IEEE*, *Member*, *CSEE*, Kailiang Zhang, and Runmin Zou, *Senior Member*, *IEEE*

***Abstract*—By considering the influence of renewable energy sources (RESs) integration on multi-area interconnected hybrid power systems, this paper proposes an equivalent input disturbance (EID)-based load frequency control (LFC) strategy, which can effectively overcome the factors of random disturbance, model uncertainties and communication delay. First, an equivalent mathematical LFC model of an interconnected system is constructed. Then, the proposed robust controllers, based on the idea of EID, are designed to suppress the randomness and volatility of the renewable energy grid connection and coordinate the frequency fluctuation of the interconnected power system. Finally, the validity and superiority of the established topology structure and the superiority of the proposed strategy are demonstrated by dynamic time domain response experiments under the condition of high penetration of renewable energy.**

***Index Terms*—Interconnected hybrid power system, LFC, renewable energy sources (RESs), robust controllers.**

## I. Introduction

An interconnected system includes independent power areas with multiple generation types connected by tie lines. LFC is usually considered as an important part of automatic generation control (AGC) for interconnected systems. With the development of renewable energy integration, such as solar energy and wind energy, its randomness and volatility bring a negative impact on the interconnected system, causing difficulties in frequency control. In order to guarantee power quality, it is very important and necessary to design an effective LFC strategy to enhance the stability of system frequency to the ideal value by considering the balance between the power generation and load consumption [1]–[3].

As a typical renewable energy source (RES), wind or solar energies are the most common sourdes in the research of power system load frequency control. Electric power systems, especially wind energy conversion systems, have been discussed over the past few decades [4]–[7]. PID and other classical controllers were often used as load frequency controllers [8], [9]. However, these controllers did not have good control performance when facing multi-source power systems containing volatile renewable energy. For a modern power system, system oscillation was more likely to expand in the system and lead to power outage. Therefore, advanced control algorithms have been widely studied in LFC, such as robust control, variable structure control, adaptive control and so on. Advanced control methods, such as fuzzy logic [10], neutral network [11], and genetic algorithm (GA) [12] can indeed improve the system performance, but these methods either need all the state information of the system or need effective online identification, which is difficult to realize in practice. In [13], a model predictive control (MPC) was proposed, which showed great robustness to the variation of governors and turbine parameters, as well as the uncertainties caused by load disturbance. A LFC method based on the flexible AC transmission system (FACTS) devices was presented for the power systems with RESs [14]. The sliding mode control (SMC) was used to deal with the uncertainties in the LFC problem [15]. [16] presented a mixed thermal system and used the bionic optimization technology to optimize controller parameters. So far, there is very little research on the LFC of interconnected systems with the coexistence of RESs under the combined influence of model uncertainties and the communication delay between areas.

An EID-based controller does not need to know the perturbation information and its design process is simple [4]. Based on the extended EID, this paper proposes a load frequency control strategy to design the controllers, which can enhance the dynamic performances for uncertain communication delay interconnected systems integrated with RESs. It can equate all disturbance information of load random disturbance, model uncertainties, communication delay, renewable energy generation fluctuation, such as wind speed fluctuation, etc., to the input end in the interconnected systems and implement compensation. The robust stability condition is analyzed by the LMI matrix, and the load frequency controllers are designed.

The remainder of this paper is organized as follows: Section II investigates the impact of the renewable energy grid connection on interconnected systems load frequency

Manuscript received November 17, 2020; revised April 8, 2021; accepted August 18, 2021. Date of online publication May 6, 2022; date of current version July 16, 2023. This research was supported in part by the NSFC of China under Grant 62373373, in part by the Natural Science Foundation of Hunan Province of China under Grant 2024JJ3033, and in part by the Science and Technology Innovation Program of Hunan Province under Grant 2022RC3051.

F. Liu, K. L. Zhang and R. M. Zou (corresponding author, email: rmzou @csu.edu.cn, ORCID: https://orcid.org/0000-0003-1747-3448) are with the School of Automation, Central South University, Changsha 410083, China.

DOI: 10.17775/CSEEJPES.2020.05590

2096-0042 © 2020 CSEE. This is an open access article under the CC BY-NC-ND license (http://creativecommons.org/licenses/by-nc-nd/4.0/).

and establishes an equivalent model of the interconnected system with PV power and doubly-fed wind turbines (DFIG). Considering the model uncertainties, stochastic fluctuation characteristics of RESs and the communication delay between multi-region interconnected systems, we design the load frequency controller based on EID for interconnected system in Section III. The implementation of the EID-based controller and the performance test are carried out in Section IV. Finally, Section V provides some conclusions.

## II. System Description and Modelling

### A. Description of The Interconnected Power System

In this section, the four-area interconnected power system is considered, where each area contains conventional thermal power units, wind power generation and PV solar power generation, as shown in Fig. 1.

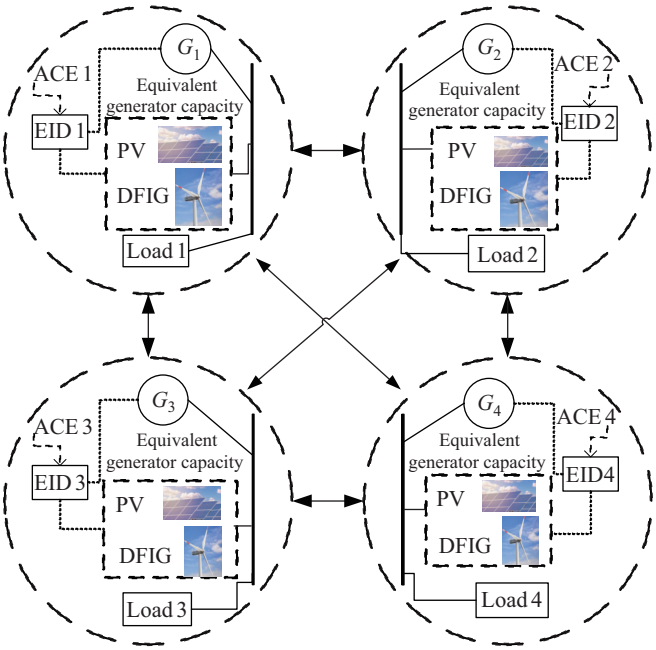


Fig. 1. Diagram of four-area interconnected hybrid power system.

### B. PV Solar Power Model

The model of solar power generation composed of a parallel string of $Ns$, which is formed by $Np$ PV cells is shown in Fig. 2. $U_{\rm DC}$ and $I_{\rm PV}$ are the output voltage and current of the solar power generation. Since the operational characteristics of PV cells are consistent, the $U_{\rm DC} - I_{\rm PV}$ mathematical model of PV power generation can be obtained by:

$$\begin{cases} I_{\rm PV} = I_{\rm ph} - I_{\rm sat}\left(\dfrac{qU_{\rm DC} + I_{\rm PV}R_s}{AKT - 1}\right) \\ I_{\rm ph} = \left(\dfrac{\Phi}{1000}\right)\left[I_{\rm SC} + k_i(T_{\rm a} - 25)\right] \end{cases} \tag{1}$$

Figure 3 shows the equivalent circuit of the PV power cell and the DC output of the PV array which varies with the solar isolation and temperature. The relevant equation for the simplified frequency response model for the PV solar power is:

$$P_{\rm PV}(t) = P_{\rm STC} \cdot \frac{J(t)}{J_{\rm STC}} \cdot [1 - \alpha \cdot \Delta T] \tag{2}$$

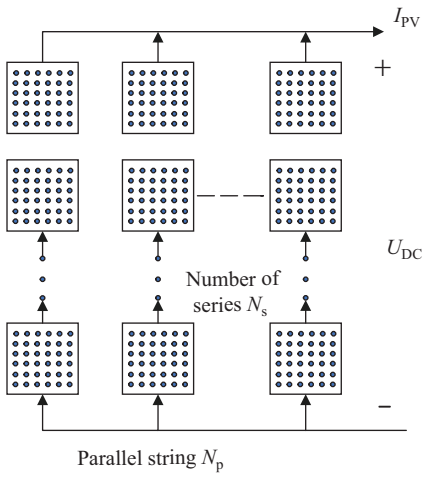


Fig. 2. Schematic diagram of PV solar power generation.

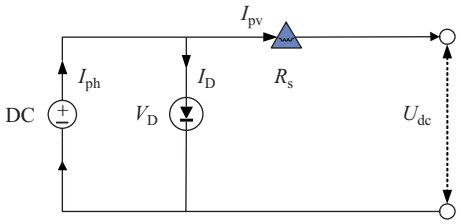


Fig. 3. Equivalent circuit of solar power cell.

where $P_{\rm STC}$ and $J_{\rm STC}$ are fixed constants, and $\Delta T$ and $\Delta J$ are the temperature coefficient and illumination coefficient.

The input of the PV boost converter is influenced by solar radiation, while the output is always influenced by load changes [17]. In order to simplify the model, the influence of temperature can be ignored for a relatively short time. The PV system transfer function is expressed by:

$$G_{\rm PV}(s) = \frac{\Delta P_{\rm PV}}{\Delta J} = \frac{1}{1 + sT_{\rm PV}} \tag{3}$$

### C. WTG Linearized Model

In practice, variable speed wind turbines has become one of the most frequently seen wind turbines in recent years. They are described in more detail in [18]. Fig. 4 displays a simplified power system model with DFIG wind turbine frequency response [4].

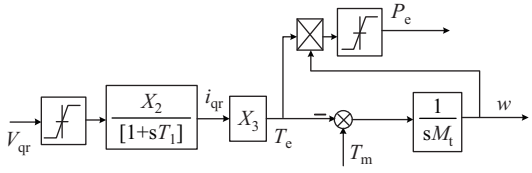


Fig. 4. Simplified frequency response model of DFIG wind turbine.

The following equations can be used to describe the structure of the DFIG model:

$$\dot{i}_{\rm qr} = -\left(\frac{1}{T_1}\right) i_{\rm qr} + \left(\frac{X_2}{T_1}\right) V_{\rm qr} \tag{4}$$

$$\dot{\omega} = -\left(\frac{X_3}{M_{\rm t}}\right) i_{\rm qr} + \left(\frac{1}{M_{\rm t}}\right) T_m \tag{5}$$

$$p_e = wX_3 i_{\rm qr} \tag{6}$$

Through linearization, Equation (6) can be rewritten as:

$$p_e = w_{\rm opt} X_3 i_{\rm qr} \tag{7}$$

and

$$T_e = i_{\rm qs} = -\frac{L_m}{L_{ss}} i_{\rm qr} = -X_3 i_{\rm qr} \tag{8}$$

where $X_2 = \frac{1}{R_{\rm r}}$, $X_3 = \frac{L_m}{L_{ss}}$ and $T_1 = \frac{L_0}{w_s R_s}$. Otherwise,

$$L_0 = L_{rr} + \frac{L_m^2}{L_{ss}},\ L_{ss} = L_s + L_m,\ L_{rr} = L_{rs} + L_m \tag{9}$$

Table I shows the meanings of the relevant parameters, and the parameters in Fig. 4 are shown in the Table II.

TABLE I
SYSTEM PARAMETERS

| Symbol | Quantity |
|---|---|
| $w_{\rm opt}$ | Rotational speed's operating point |
| $T_e$ | Electromagnetic torque |
| $T_m$ | Mechanical power change |
| $w$ | Rotational speed |
| $P_e$ | Wind turbine's active power |
| $i_{qr}$ | Rotor current's Q-axis component |
| $V_{qr}$ | Rotor voltage's Q-axis component |
| $M_t$ | Wind turbine's equivalent inertia constant |
| $L_m$ | Magnetizing inductance |
| $L_r$ | Rotor's inductance |
| $L_s$ | Stator's leakage inductance |
| $L_{rr}$ | Rotor's self-inductance |
| $L_{ss}$ | Stator's self-inductance |
| $w_s$ | Synchronous speed |

TABLE II
WIND TURBINE PARAMETERS AND OPERATING POINT

| Symbol | Quantity | Value (p.u.) |
|---|---|---|
| $R_r$ | Magnetizing inductance | 0.3 |
| $R_s$ | Stator resistances | 0.1 |
| $X_{lr}$ | – | 0.05 |
| $X_{ls}$ | – | 1.0 |
| $X_m$ | – | 21.0 |
| $M_t$ | Equivalent inertia constant of wind turbine | 10.0 |

Based on the simplified frequency model of DFIG shown in Fig. 4, the equivalent pattern of the grid-connected DFIG can be obtained. The equivalent parameters are calculated by:

$$\begin{cases} S_{\rm eq} = \sum_{i=1}^{N} S_i, & \delta_i = S_i / \sum_{i=1}^{N} S_i \\ X_{\rm eq} = \sum_{i=1}^{N} \delta_i X_i, & C_{\rm eq} = \frac{1}{N} \sum_{i=1}^{N} C_i \end{cases} \tag{10}$$

in which $S$ is the wind turbine capacity; $\delta$ is for the capacity weighting coefficient; $X$ represents other generator parameters; $C$ represents wind energy utilization.

### D. The LFC System Model

Since different areas of the power systems are connected to each other by contact lines or high-voltage transmission lines, the frequency variation of each individual area will affect the frequency of the interconnected region, so the frequency control system in any area of the four-area hybrid power system must restrain the power exchanged between areas and the frequency of the area [14]. Power signals of tie lines are considered in the dynamic frequency control model, as shown in Fig. 5.

To sum up, the matrix form of the dynamic equation of each area can be uniformly expressed by:

$$\dot{x}_i(t) = A_i x_i(t) + B_i u_i(t) + \sum_{j \in N, j \neq i} E_{ij} x_j(t) + F_i \Delta P_{di}(t) \tag{11}$$

In fact, the balance point is always changed with the load change. This causes the system parameters to be uncertain. To describe the power system more accurately, the equation (11) can be expressed as:

$$\begin{cases} \dot{x}_i(t) = (A_i + \Delta A_i(t)) x_i(t) + (A_{di} + \Delta A_{di}(t)) x_i(t - h_i) \\ \qquad + (B_i + \Delta B_i(t)) u_i(t) + \sum_{j \in N, j \neq i} E_{ij} x_j(t) \\ \qquad - F_i(\Delta P_{di}(t) + \Delta P_{\rm RESsi}(t)) \\ y = C_i x_i(t) \end{cases} \tag{12}$$

where the state $x_i(t)$ is equal to $[\Delta f_i \ \ \Delta P_{mi} \ \ \Delta P_{vi} \ \ \Delta E_i \ \ \Delta P_{tie}^{ij} \ \ \Delta i_{qri} \ \ \Delta w_i \ \ \Delta P_{PVi}] \in R_{\rm n}$ and $\Delta \dot{E}_i = ACE_i = \Delta P_{tie,i} + \beta_i \Delta f_i$, is the control vector, $\Delta P_{di}$ and $\Delta P_{\rm RESs}$ are the perturbation vector and Renewable energy generation fluctuation, $A_i \in R^{ni \times ni}$, $B_i \in R^{ni \times mi}$, $C_i \in R^{ni \times mi}$, $E_{ij} \in R^{ni \times mi}$, $F_i \in R^{ni \times mi}$, are constant value matrices of the system with appropriate dimensions, $\Delta A_i(t)$, $\Delta A_{di}(t)$ and $\Delta B_i(t)$ are parameter uncertainties with the general form in (13), $h_i$ is the time delay of the communication signal.

$$[\Delta A_i(t) \ \ \Delta B_i(t) \ \ \Delta A_{di}(t)] = MN(t)[E_{ai} \ \ E_{bi} \ \ E_{di}] \tag{13}$$

where the matrices $M$, $E_{ai}$, $E_{bi}$, $E_{di}$ are known; and the matrix $N(t)$ is unknown when satisfying $N^{\rm T}(t)N(t) \leq I$, $\forall t > 0$ with its elements being the Lebesgue measurable.

## III. PROPOSED FREQUENCY CONTROL METHOD

This section is devoted to designing the load frequency controller based on EID to constitute the control system of the studied multi-source interconnected power system. The original EID method cannot be directly applied to the system with uncertain parameters or communication delay, because these factors cause the controller parameters to couple with each other and the separation principle is no longer effective. Therefore, we extend this method to the system with uncertainties and communication delay [19], a new design framework is proposed for the studied interconnected power system with model uncertainties and communication delay. The closed-loop system model is established by using three states contained in the control structure, so both SF controller and state observer gains can be obtained.

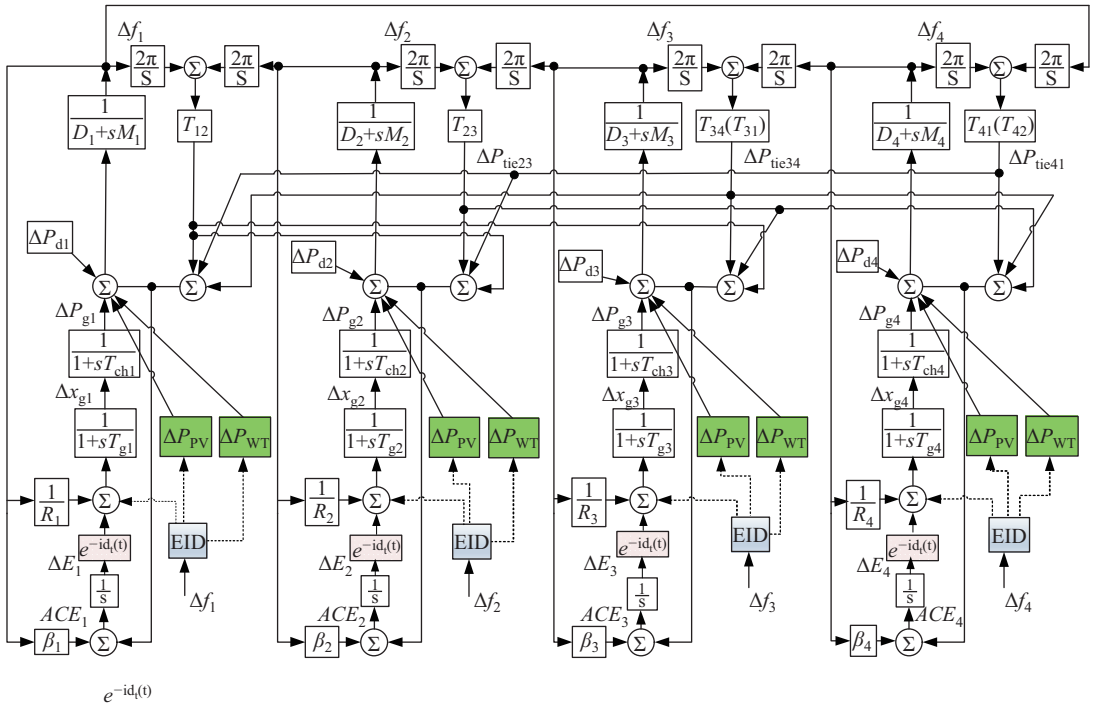


Fig. 5. LFC model of the studied four-area renewable energy sources integrated interconnected hybrid power system.

### A. Description of EID

The EID method was proposed by She [20] and later introduced into the field of power system load frequency control [4]. The EID's idea is that the disturbance, $w_e(t)$ in Fig. 6(b), has a similar influence for the system, while the practical external disturbance $w(t)$ is as shown in Fig. 6(a). It can be used to reversely compensate the control input channel. Therefore, the disturbance $w_e(t)$ is considered as an equivalent input signal for actual disturbance. Both the prior information of disturbance and the inverse dynamics of plants are not required [21].

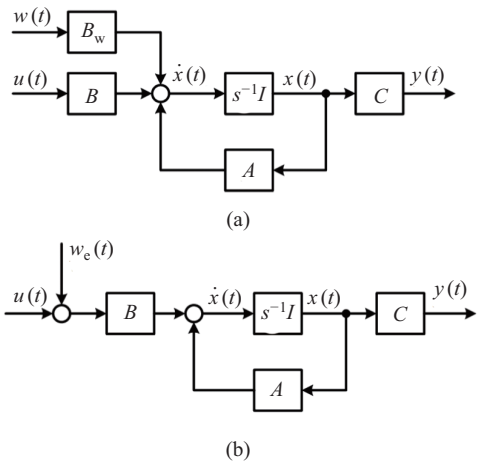


Fig. 6. The core point of EID. (a) Plant with disturbance. (b) Plant with EID compensation.

According to the above, parameter uncertainties are described as a state and input-dependent disturbance. Assuming a disturbance, $w_{ei}(t)$ is imposed only on the control input channel, and it has a similar influence for output like $\Delta A_i(t)x_i(t) + \Delta A_{di}(t)x_i(t-h_i) + \Delta B_i(t)u_i(t) + \sum_{j\in N, j\neq i} E_{ij}x_j(t) - F_i(\Delta P_{di}(t) + \Delta P_{\mathrm{RESsi}}(t))$. In addition, in the described multi-region power system, there may be multiple delay quantities $h_i$, which are considered to be equal for simplification of the analysis, then any area's plant for this interconnected hybrid power system can be decomposed as:

$$\begin{cases} \dot{x}_i(t) = A_i x_i(t) + A_{di} x_i(t-h) + B_i(u_i(t) + w_{ei}(t)) \\ y_i(t) = C_i x_i(t) \end{cases} \tag{14}$$

where $w_{ei}(t) = [\Delta P_{di} \Delta T_m \Delta V_i]^{\mathrm{T}}$, $\Delta T_m$ represent wind speed fluctuation and $\Delta V_i$ represent the area interface quantity.

Then, system (14) is used to design the EID-based controller, in which we construct a closed-loop control structure as shown in Fig. 7 based on EID's idea. We can obtain the RESs fluctuation information and the external random disturbance information through the full-dimension state observer. Moreover, we can flexibly process the disturbance information and compensate the disturbance by the disturbance estimator, and then improve the frequency control performance of the whole system. Using a single area as an example, we design the controller as shown in part B.

### B. Configuration of EID-based Controller

According to the influence of the doubly-fed wind power generator speed deviation effect, tie line power deviation, load disturbance and the PV power fluctuations, we define a equivalent input disturbance from the outside world, through the state observer to estimate and reverse compensation and realize the effective disturbance suppression.

Figure 7 shows the LFC system structure of an EID-based renewable energy integrated power system, and it includes 4

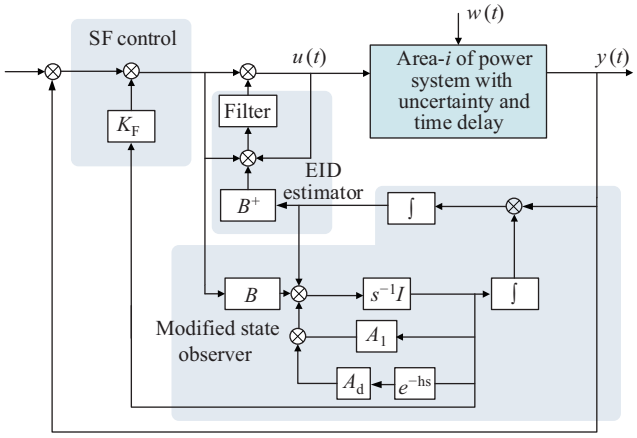


Fig. 7. The closed-loop control structure of each area based on EID.

parts: a full-dimension state observer, an EID estimator, the controlled object, and a state-feedback(SF) controller. $\Delta f_{\text{ref}}$ is the frequency deviation reference value of the closed-loop system and $K_F$ is the SF gain.

The inputs of the observer are $u(t)$ and $y(t)$ of the closed-loop control power system. The observer state space is expressed as:

$$\begin{cases} \dot{\hat{x}}(t) = A\hat{x}(t) + A_d\hat{x}(t-h) + Bu_f(t) + \Psi(y(t) - \hat{y}(t)) \\ \hat{y}(t) = C\hat{x}(t) \end{cases} \tag{15}$$

The state is a reconstruction of. For EID estimator,

$$B^+ = (B^{\mathrm{T}}B)^{-1}B^{\mathrm{T}} \tag{16}$$

$$\Delta x = \hat{x}(t) - x(t) \tag{17}$$

Similar to [19], there is:

$$\hat{w}(t) = B^+LC[x(t) - \hat{x}(t)] + u_f(t) - u(t) \tag{18}$$

where $\hat{w}(t)$ represents the estimated value of load disturbance.

The noise contained in $\tilde{w}(t)$ will affect the control performance, so a filter is adopted to suppress it:

$$\begin{cases} \dot{x}_F(t) = A_F x_F(t) + B_F\hat{w}(t) \\ \tilde{w}(t) = C_F x_F(t) \end{cases} \tag{19}$$

Since measurement noise is inevitable in the output, $F(s)$ is employed to choose an appropriate angular frequency bandwidth for interference estimation, and is obtained as:

$$\tilde{W}(s) = F(s)\hat{W}(s) \tag{20}$$

where $\tilde{W}(s)$ and $\hat{W}(s)$ are Laplace transforms of $\tilde{w}(s)$ and $\hat{w}(s)$, respectively. The control law is:

$$u(t) = u_f(t) - \tilde{w}(t) \tag{21}$$

### C. Optimal Design of Controller Parameters

Let $w(t) = 0$. Then, the plant studied is:

$$\begin{cases} \dot{x}_i(t) = (A_i + \Delta A_i(t))x_i(t) \\ \qquad + (A_{di} + \Delta A_{di}(t))x_i(t - h_i) \\ \qquad + (B_i + \Delta B_i(t))u_i(t) \\ \qquad + \sum_{j\in N, j\neq i} E_{ij}x_j(t) \\ y = C_i x_i(t) \end{cases} \tag{22}$$

An infinite horizon quadratic cost function is:

$$J = \int_0^\infty [x^{\mathrm{T}}(t)Rx(t) + u^{\mathrm{T}}(t)Qu(t)]\mathrm{d}t \tag{23}$$

where $R$ and $Q$ are given positive definite symmetric matrices.

Since there are three state variables, $\hat{x}(t), \Delta x(t), x_F(t)$ in Fig. 7, define as follows:

$$\varphi(t) = [\hat{x}^{\mathrm{T}}(t) \quad \Delta x^{\mathrm{T}}(t) \quad x_F^{\mathrm{T}}(t)]^{\mathrm{T}} \tag{24}$$

then the closed-loop power system is described as:

$$\begin{aligned} \dot{\hat{x}}(t) &= A\hat{x}(t) + A_d\hat{x}(t-h) + Bu_f(t) + LC\Delta x(t) \\ \Delta\dot{x}(t) &= (A - LC + \Delta A)\Delta x(t) + (A_d + \Delta A_d)\Delta x(t-h) \\ &\quad + \Delta Bu_f(t) - [B + \Delta B]C_F x_F(t) \\ &\quad + \Delta A\hat{x}(t) + \Delta A_d\hat{x}(t-h) \\ \dot{x}_F(t) &= A_F x_F(t) + B_F B^+ LC\Delta x(t) + B_F C_F x_F(t). \end{aligned}$$

So, we can obtain the system state-space model:

$$\begin{aligned} \dot{\varphi}(t) = &(\bar{A} + \Delta\bar{A})\varphi(t) + (\bar{A}_d + \Delta\bar{A}_d)\varphi(t-h) \\ &+ (\bar{B} + \Delta\bar{B})u_f(t) \end{aligned} \tag{25}$$

where

$$\bar{A} = \begin{bmatrix} A & LC & 0 \\ 0 & A - LC & -BC_F \\ 0 & B_F B^+ LC & A_F + B_F C_F \end{bmatrix},\ \bar{B} = \begin{bmatrix} B \\ 0 \\ 0 \end{bmatrix}$$

$$\bar{A}_d = \mathrm{diag}\{A_d \quad A_d \quad 0\}.\ \Delta\bar{A} = \begin{bmatrix} 0 & 0 & 0 \\ \Delta A & \Delta A & -\Delta BC_F \\ 0 & 0 & 0 \end{bmatrix}$$

$$\Delta\bar{A}_d = \begin{bmatrix} 0 & 0 & 0 \\ \Delta A_d & \Delta A_d & 0 \\ 0 & 0 & 0 \end{bmatrix},\ \Delta\bar{B} = \begin{bmatrix} 0 \\ \Delta B \\ 0 \end{bmatrix}$$

where

$$[\Delta\bar{A}(t)\Delta\bar{B}(t)\Delta\bar{A}_d(t)] = \bar{M}N(t)[\bar{E}_{\mathrm{a}} \quad \bar{E}_{\mathrm{b}} \quad \bar{E}_d] \tag{26}$$

$$\bar{M} = [0 \quad D^{\mathrm{T}} \quad 0]^{\mathrm{T}}\bar{E}_{\mathrm{a}} = [E_{\mathrm{a}} \quad E_{\mathrm{a}} \quad -E_{\mathrm{b}}C_F] \tag{27}$$

$$\bar{E}_{\mathrm{b}} = E_{\mathrm{b}},\ \bar{E}_d = [E_d \quad E_d \quad 0] \tag{28}$$

The SF control law can be obtained as:

$$u_f(t) = \bar{K}\varphi(t) \tag{29}$$

in which:

$$\bar{K} = [K_F \quad 0 \quad 0] \tag{30}$$

### D. Stability Analysis

Assume the output matrix $C$ can be decomposed as:

$$C = \mathrm{V}[\hat{S} \quad 0]\hat{T}^{\mathrm{T}}, \tag{31}$$

where the matrix $\hat{S}$ is a positive-definite, and the matrices $V$ and $\hat{T}^{\mathrm{T}}$ are unitary. $\hat{T}$ is:

$$\hat{T} = [T_1 \quad T_2]. \tag{32}$$

Based on Lemma 1 and Lemma 2 in [19], a low conservative stability criterion for the interconnected power system with uncertainty and time delay is oabtained.

**Theorem 1**. Given two matrices $R > 0$ and $Q > 0$, If there are symmetric positive-definite matrices $Y_1, Y_2, Y_3, X_1, X_{11},$

$X_{22}, X_3$ and two appropriate matrices $W$, $W_1$, the following linear matrix inequality (LMI) is feasible. For a constant $\varepsilon > 0$, the time-delay power system (12) is asymptotically stable for any constant time delay $h > 0$ under the control law (29).

$$\begin{bmatrix} \Psi_{11} & \Psi_{12} & \Psi_{13} & \Psi_{14} & \Psi_{15} & \Psi_{16} \\ * & -\Psi_{22} & \Psi_{23} & 0 & 0 & 0 \\ * & * & -\varepsilon I & 0 & 0 & 0 \\ * & * & * & -R^{-1} & 0 & 0 \\ * & * & * & * & -Q^{-1} & 0 \\ * & * & * & * & * & -\Psi_{22} \end{bmatrix} < 0 \quad (33)$$

$$\boldsymbol{\Psi}_{11} = \begin{bmatrix} \Phi_{11} & WC & 0 \\ * & \Phi_{22} & \Phi_{23} \\ * & * & \Phi_{33} \end{bmatrix}$$

$$\boldsymbol{\Phi}_{11} = A_1X_1 + BW_1 + X_1A_1^{\mathrm{T}} + W_1^{\mathrm{T}}B^{\mathrm{T}}$$

$$\boldsymbol{\Phi}_{22} = A_1X_2 + X_2A_1^{\mathrm{T}} - WC - C^{\mathrm{T}}W^{\mathrm{T}} + \varepsilon MM^{\mathrm{T}}$$

$$\boldsymbol{\Phi}_{23} = C^{\mathrm{T}}W^{\mathrm{T}}B^{+\mathrm{T}}B_F^{\mathrm{T}} - BC_FX_3$$

$$\boldsymbol{\Phi}_{33} = X_3A_F^{\mathrm{T}} + A_FX_3 + B_FC_FX_3 + X_3C_F^{\mathrm{T}}B_F^{\mathrm{T}}$$

$$\boldsymbol{\Psi}_{12} = \begin{bmatrix} A_dY_1 & 0 & 0 \\ 0 & A_dY_2 & 0 \\ 0 & 0 & 0 \end{bmatrix}, \ \boldsymbol{\Psi}_{13} = \begin{bmatrix} X_1E_1^{\mathrm{T}} + W_1^{\mathrm{T}}E_2^{\mathrm{T}} \\ X_2E_1^{\mathrm{T}} \\ -X_3C_F^{\mathrm{T}}E_2^{\mathrm{T}} \end{bmatrix}$$

$$\boldsymbol{\Psi}_{14} = \begin{bmatrix} X_1 & & \\ & X_2 & \\ & & X_3 \end{bmatrix}, \ \boldsymbol{\Psi}_{15} = \begin{bmatrix} W_1^{\mathrm{T}} \\ 0 \\ 0 \end{bmatrix}$$

$$\boldsymbol{\Psi}_{16} = \Psi_{14}$$

$$\boldsymbol{\Psi}_{22} = \begin{bmatrix} Y_1 & & \\ & Y_2 & \\ & & Y_3 \end{bmatrix}, \ \boldsymbol{\Psi}_{23} = \begin{bmatrix} Y_1E_d^{\mathrm{T}} \\ Y_2E_d^{\mathrm{T}} \\ 0 \end{bmatrix}$$

The cost function meets the condition (34),

$$J \le \varphi^{\mathrm{T}}(0)P\varphi(0) + \int_{-h}^{0} \varphi^{\mathrm{T}}(s)S\varphi(s)\mathrm{d}s \quad (34)$$

$$X_2 = [T_1 \ \ T_2] \begin{bmatrix} X_{11} & 0 \\ 0 & X_{22} \end{bmatrix} \quad (35)$$

The SF controller gain and the observer gain are solved by:

$$K_F = W_1X_1^{-1}, \ L = WV\hat{S}X_{11}^{-1}\hat{S}^{-1}V^{\mathrm{T}} \quad (36)$$

Reference [19] shows a detailed proof of this Theorem, so the processes of additional proof are omitted here.

## IV. Simulation Studies

Through simulation experiments, four-area interconnected systems with EID-based load frequency controllers are established to verify its effectiveness and superiority, which has solar and wind energy for each area. Different load variations are used to test the control performance of EID allocated to different areas. Some main parameter selections are given in Table III.

First, the random load variation suppression ability with renewable uncertainties and communication delay of the proposed EID-based controller is verified. The variation range of the system parameters in Area-2 is $H_w \in [6 \ \ 12]$, $H_{\mathrm{opt}} \in [0.97 \ \ 1.37]$, $T_{\mathrm{PV}} \in [1.0 \ \ 2.6]$. The communication time delay is set to equal 0.2 s. In Fig. 8(a), when Area-2 suffers random load variation disturbance, frequency fluctuations of the four-area systems with or without EID controllers are demonstrated from Fig. 8(b) to Fig. 8(c). Two cases are studied with/without EID controllers respectively. It can be found that the frequency curves of the power system are very unstable without the controller, while the frequency could approach zero under the actions of the EID controller. We can also see that under EID-based controllers, the frequency fluctuation of Area-2 can be

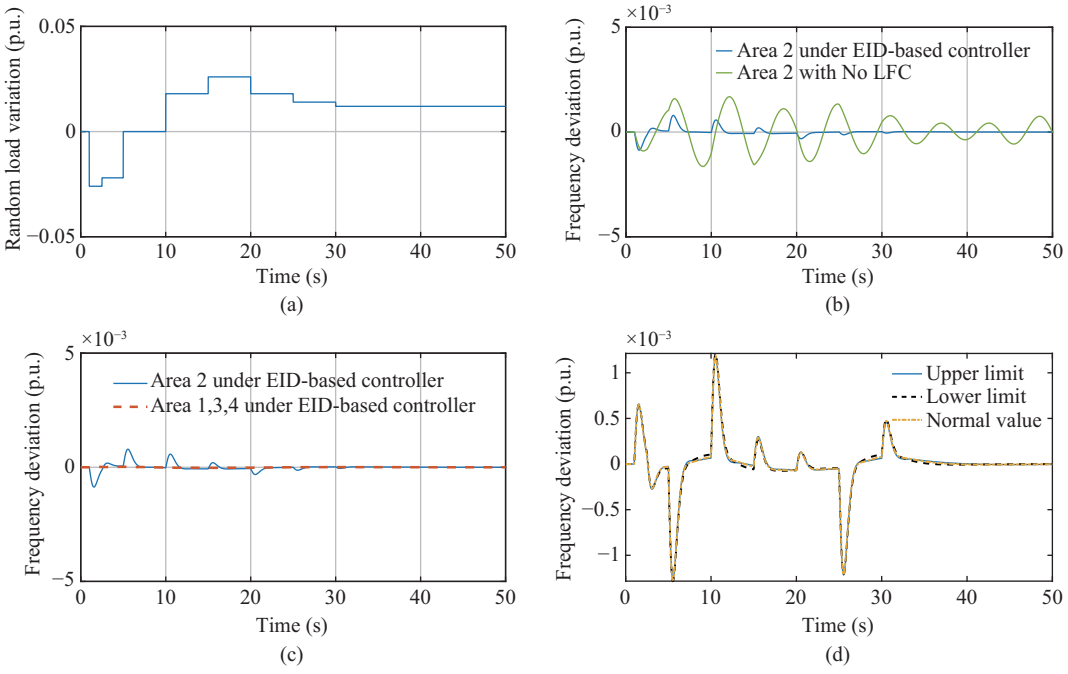


Fig. 8. Dynamic response of power system. (a) Load disturbance applied to Area-2. (b) Frequency deviation of Area-2 with EID-based controllers and No controller. (c) Frequency response of four areas under EID-based controllers. (d) Frequency fluctuation of different system parameters of Area-2 under EID controller.

TABLE III
PARAMETERS OF FOUR CONTROL AREAS

| Symbol | Quantity | Area1 | Area2 | Area3 | Area4 |
|---|---|---|---|---|---|
| $T_{\rm ch}$ (s) | Thermal power unit governor time constant | 0.3 | 0.4 | 0.1 | 0.4 |
| $T_{\rm g}$ (s) | Steam turbine time constant | 0.1 | 0.17 | 0.1 | 0.17 |
| $R_i$ (p.u.) | Speed droop coefficient of Area-$i$ | 0.05 | 0.05 | 0.05 | 0.05 |
| $D_i$ (p.u.) | Equivalent damping coefficient of Area-$i$ | 1.0 | 1.5 | 1.0 | 1.5 |
| $M_i$ (p.u.) | Inertia constant of generator of Area-$i$ | 10 | 12 | 10 | 12 |
| $T_{\rm PV}$ (p.u.) | Temperature coefficient of PV modules | 1.8 | 1.3 | 1.8 | 1.3 |

damped in the range of $[-5\ \ 5]\times10^{-3}$ pu and the frequency fluctuations of other areas are almost negligible, as shown in Fig. 8(c). It should also be emphasized that the EID controller is insensitive to the parameter uncertainties and can effectively improve the system stability in Fig. 8(d).

Then the superiority of the EID-based controller is studied. In Fig. 9, the different load variations are shown to measure the control effects while the EID-based controllers are allocated to different areas. The dynamic responses of the renewable energy integrated uncertain time-delay system equipped with fuzzy PID controllers, MPC controllers or EID-based controllers are demonstrated in Fig. 10, respectively. Fig. 10(a)-(d) show the response curves of each area under different controllers, it can be determined that the designed EID-based controllers have smaller overshoot, faster adjustment speed and better robustness compared with fuzzy tuning PID controllers and MPC controllers. The simulation results in Fig. 10 indicate that the EID-based controllers can estimate and compensate the disturbances, have good dynamic performance, and can control different types of random load disturbances in the studied renewable energy integrated power system.

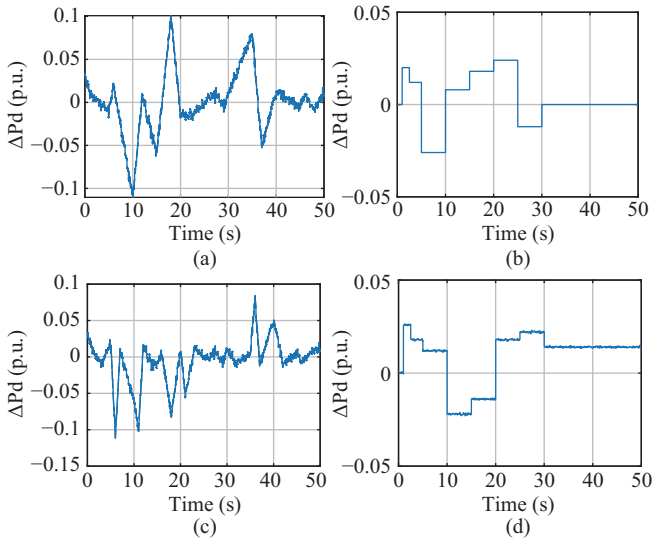


Fig. 9. Load power variations of four areas. (a) Area-1. (b) Area-2. (c) Area-3. (d) Area-4.

Figure 11(a) shows the PV power generation in four areas under the EID controllers, and Fig. 11(b) shows the rotor speed deviation of doubly-fed wind turbines in the four regions under the EID controllers. The simulation results indicate EID-based controllers have better regulation effects for renewable energy. Moreover, we can see from Fig. 12 that the controller can maintain better control performance and effectively eliminate the area control error (ACE).

## V. CONCLUSION

Aiming at overcoming the negative impact of large-scale uncertain renewable energy power connections on the stability and security of power systems, and on the consideration of the influence of renewable energy randomness and volatility on

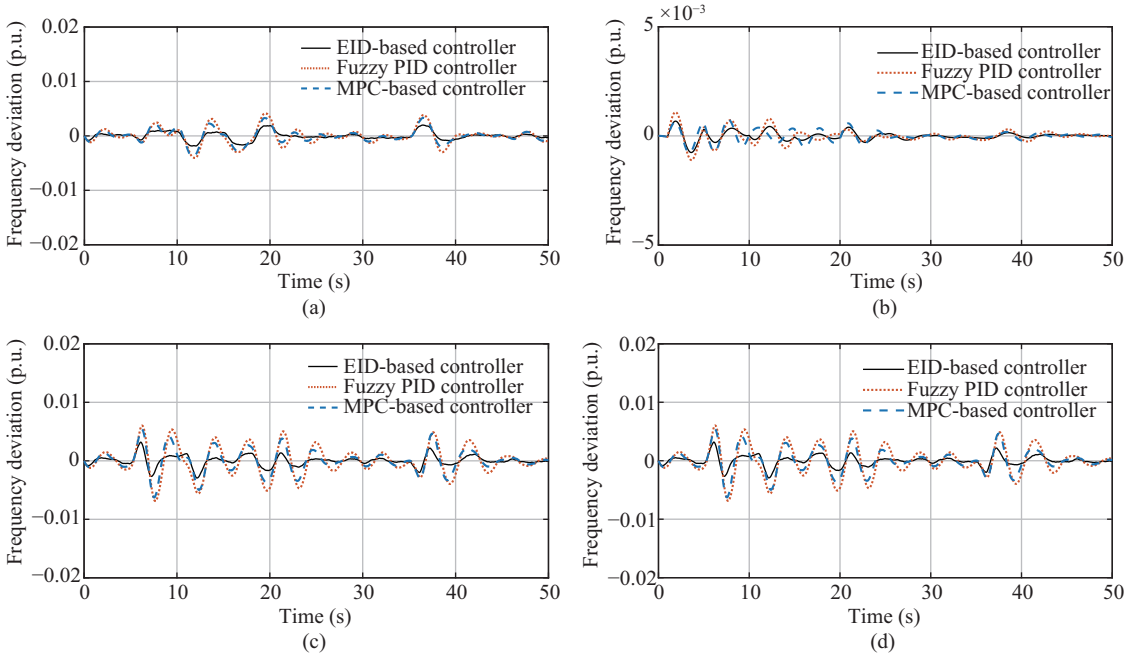


Fig. 10. Dynamic frequency deviations with different controller under suffered load power variations. (a) Area-1. (b) Area-2. (c) Area-3. (d) Area-4.

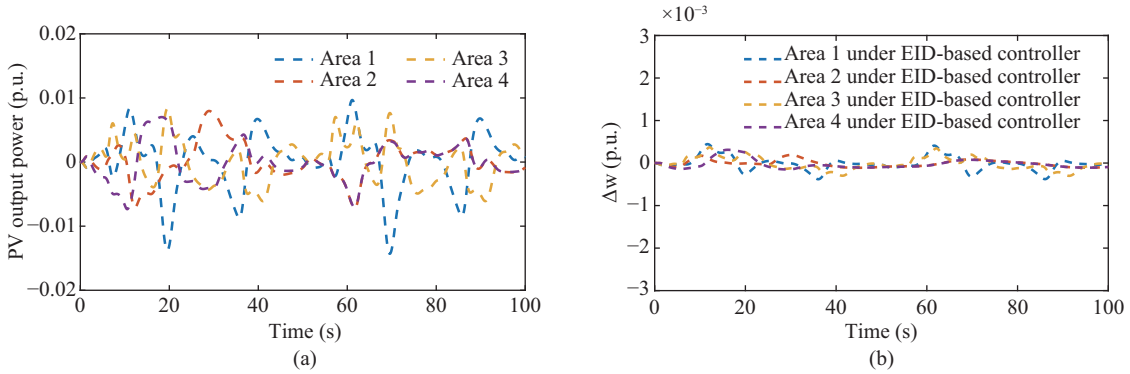


Fig. 11. Renewable energy regulation signals. (a) Output power of the PV model under EID-based controller. (b) Wind turbine rotor speed deviation of four areas.

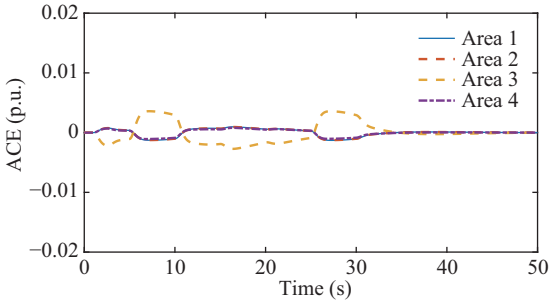


Fig. 12. Area control error of power system under EID-based controllers.

this system, EID-based controllers are presented in this paper to maintain the frequency stability of four-area interconnected hybrid power systems integrated with RESs. Against the established uncertain renewable energy integrated four-area

interconnected system load frequency control to design an EID-based LFC controller, the LFC model is set up and experimental results indicate the validity and superiority of the proposed controller. It is obvious that the proposed EID-based controllers have great robustness and stability, can effectively and quickly prevent the influence of external random disturbance, model uncertainties, renewable energy and communication delay on power system frequency stability.

## REFERENCES

[1] Z. M. Yan and Y. Xu, "Data-driven load frequency control for stochastic power systems: a deep reinforcement learning method with continuous action search," *IEEE Transactions on Power Systems*, vol. 34, no. 2, pp. 1653–1656, Mar. 2019.

[2] C. G. Li, Y. Wu, Y. L. Sun, H. X. Zhang, Y. T. Liu, Y. L. Liu, and V. Terzija, "Continuous under-frequency load shedding scheme for power system adaptive frequency control," *IEEE Transactions on Power Systems*, vol. 35, no. 2, pp. 950–961, Mar. 2020.

[3] Q. Hui, J. L. Yang, X. Yang, Z. Chen, Y. Li, and Y. Teng, "A robust control strategy to improve transient stability for AC-DC interconnected power system with wind farms," *CSEE Journal of Power and Energy Systems*, vol. 5, no. 2, pp. 259–265, Jun. 2019.

[4] F. Liu and J. J. Ma, "Equivalent input disturbance-based robust LFC strategy for power system with wind farms," *IET Generation, Transmission & Distribution*, vol. 12, no. 20, pp. 4582–4588, Nov. 2018.

[5] S. J. Song Z. Wei, Y.Z. Lin and B. Liu, "Impedance Modeling and Stability Analysis of PV Grid-connected Inverter Systems Considering Frequency Coupling," *CSEE Journal of Power and Energy Systems*, vol. 6, no. 2, pp. 279–290, Jun. 2020.

[6] C. X. Mu, Y. F. Tang, and H. B. He, "Improved sliding mode design for load frequency control of power system integrated an adaptive learning strategy," *IEEE Transactions on Industrial Electronics*, vol. 64, no. 8, pp. 6742–6751, Aug. 2017.

[7] C. Chen, Y. Q. Bao, X. H. Wu, and B. B. Wang, "Incremental cost consensus algorithm for on/off loads to enhance the frequency response of the power system," *IEEE Access*, vol. 8, pp. 67687–*67697, Apr. 2020*.

[8] *A. Abazari, H. Monsef,* and B. Wu, "Load frequency control by de-loaded wind farm using the optimal fuzzy-based PID droop controller," *IET Renewable Power Generation*, vol. 13, no. 1, pp. 180–190, Jan. 2019.

[9] *S.Y.Chen, Q.F. Yang, J.Y. Zhou and X. Chen. "A Model Predictive Control Method for Hybrid Energy Storage Systems," CSEE Journal of Power and Energy Systems*, vol. 7, no. 2, pp.329–338, Mar. 2021.

[10] G. G. Chen, Z. J. Li, Z. Z. Zhang, and S. Y. Li, "An improved ACO algorithm optimized fuzzy PID controller for load frequency control in multi area interconnected power systems," *IEEE Access*, vol. 8, pp. 6429–6447, 2020.

[11] M. K. Debnath, R. Agrawal, S. R. Tripathy, and S. Choudhury, "Artificial neural network tuned PID controller for LFC investigation including distributed generation," *International Journal of Numerical Modelling: Electronic Networks, Devices and Fields*, vol. 33, no. 5, pp. e2740, Sep./Oct. 2020.

[12] E. Cam, G. Gorel, and H. Mamur, "Use of the genetic algorithm-based fuzzy logic controller for load-frequency control in a two area interconnected power system," *Applied Sciences*, vol. 7, no. 3, pp. 308, Mar. 2017.

[13] J. Z. Liu, Q. Yao, and Y. Hu, "Model predictive control for load frequency of hybrid power system with wind power and thermal power," *Energy*, vol. 172, pp. 555–565, Apr. 2019.

[14] A. Dutta and S. Prakash, "Load frequency control of multi-area hybrid power system integrated with renewable energy sources utilizing FACTS & energy storage system," *Environmental Progress & Sustainable Energy*, vol. 39, no. 2, pp. e13329, Mar. 2020.

[15] A. Dev and M. K. Sarkar, "Robust higher order observer based non-linear super twisting load frequency control for multi area power systems via sliding mode," *International Journal of Control, Automation and Systems*, vol. 17, no. 7, pp. 1814–1825, Jul. 2019.

[16] A. Rahman, C. L. Saikia, and N. sinha, "Automatic generation control of an interconnected two-area hybrid thermal system considering dish-stirling solar thermal and wind turbine system," *Renewable Energy*, vol. 105, pp. 41–54, May 2017.

[17] A. S. Jeddi, S. H. Abbasi, and F. Shabaninia, "Load frequency control of two area interconnected power system (Diesel Generator and Solar PV) with PI and FGSPI controller," in *CSI International Symposium on Artificial Intelligence & Signal Processing*, Shiraz, Iran, pp. 526–531, May 2012.

[18] R. Azizipanah-Abarghooee, M. Malekpour, T. Dragičević, F. Blaabjerg, and V. Terzija, "A linear inertial response emulation for variable speed wind turbines," *IEEE Transactions on Power Systems*, vol. 35, no. 2, pp. 1198–1208, Mar. 2020.

[19] F. Gao, M. Wu, P. Yu, and X. Chen, "Guaranteed cost control for

uncertain time-delay systems with persistent disturbances," in *2016 35th Chinese Control Conference*, Chengdu, China, pp. 3017–3022, Jul. 2016.
[20] J. H. She, M. X. Fang, Y. Ohyama, H. Hashimoto, and M. Wu, "Improving disturbance-rejection performance based on an equivalent-input-disturbance approach," *IEEE Transactions on Industrial Electronics*, vol. 55, no. 1, pp. 380–389, Jan. 2008.
[21] Y. W. Du, W. H. Cao, J. H. She, M. Wu, M. X. Fang, and S. Kawata, "Disturbance rejection and control system design using improved equivalent input disturbance approach," *IEEE Transactions on Industrial Electronics*, vol. 67, no. 4, pp. 3013–3023, Apr. 2020.

**Fang Liu** received a B.Eng. degree in Automatic Control from Zhengzhou University of Light Industry, Zhengzhou, China in 2005 and a Ph.D. degree in Power System Control from Waseda University, Japan in 2011. Since 2017, she is a Full Professor in the School of Automation, CSU, Changsha, China. Her main research interests include power system stability and control, robust control, smart grid.

**Kailiang Zhang** received a B.S. degree from the School of Information and Electrical Engineering, Shandong Jianzhu University, Jinan, China, in 2018. He is working toward an M.S. degree in the School of Automation, Central South University, Changsha, China. His main research interests include power system load frequency control and inverter technology.

**Runmin Zou** received a B.Eng. degree in Automatic Control and an M.Eng. degree in Control Theory and Control Engineering from the Central South University (CSU), Changsha, China, in 1994 and 1997, respectively, and a Ph.D. degree in Automatic Control from the Ecole Centrale de Nantes, Nantes, France, in 2009. Since 1997, he has been with the School of Automation, CSU, where he is currently a Full Professor. His main research interests include the intersection of control theory, artificial intelligence and power electronics with their applications to renewable energy, and complex dynamical systems.